



# Geophysical Research Letters®



## RESEARCH LETTER

10.1029/2022GL102302

## High-Resolution Records of Millennial-Scale East Asian Winter Monsoon in the Shelf Sea of Eastern China

Yong Shi<sup>1,2</sup>, Xiaomei Xu<sup>1</sup>, Guang Yang<sup>1</sup>, Jiabi Du<sup>3</sup>, Jixuan Lv<sup>1</sup>, Shuo Zhang<sup>1</sup>, Shengjing Liu<sup>1</sup>, Tao Liu<sup>1</sup>, Zhenyu Zhang<sup>1</sup>, Shu Gao<sup>1</sup> , and Jianhua Gao<sup>1,2,4</sup> 

<sup>1</sup>School of Geography and Ocean Science, Ministry of Education Key Laboratory for Coast and Island Development, Nanjing University, Nanjing, China, <sup>2</sup>Frontiers Science Center for Critical Earth Material Cycling, Nanjing University, Nanjing, China, <sup>3</sup>Virginia Institute of Marine Science, College of William and Mary, Gloucester Point, VA, USA, <sup>4</sup>Laboratory for Marine Geology, Qingdao National Laboratory for Marine Science and Technology, Qingdao, China

### Key Points:

- A link between cross-front transport and the East Asian winter monsoon (EAWM) was found in the shelf sea, and the leaked sediment was used to reconstruct the EAWM
- The wind speed of the EAWM since 4.4 ka was quantitatively reconstructed at high resolution (~5 yr) for the first time
- Correlation between the EAWM and the temperature on the centennial scale since ~2.0 ka was reversed by the increasing CO<sub>2</sub> at the Current Warm Period

### Supporting Information:

Supporting Information may be found in the online version of this article.

### Correspondence to:

J. Gao,  
jhgao@nju.edu.cn

### Citation:

Shi, Y., Xu, X., Yang, G., Du, J., Lv, J., Zhang, S., et al. (2023). High-resolution records of millennial-scale East Asian winter monsoon in the shelf sea of eastern China. *Geophysical Research Letters*, 50, e2022GL102302. <https://doi.org/10.1029/2022GL102302>

Received 29 NOV 2022  
Accepted 20 MAR 2023

**Abstract** The evolution of the East Asian winter monsoon (EAWM) during the Holocene remains controversial because of the lack of reliable proxies. In this study, a link between cross-front transport and the EAWM was found in the North Yellow Sea, and the EAWM intensity could be imprinted in the leaked sediment, which permits reliable reconstruction of the EAWM on well-preserved offshore deposition. By comparison with instrumental data, the wind speed of the EAWM since 4.4 ka was quantitatively reconstructed for the first time at high resolution (~5 yr). The results show that the EAWM gradually weakened in the mid-to-late Holocene, which was likely controlled by solar insolation, and that there has been a negative relationship between the EAWM and temperature on the centennial scale since ~2.0 ka; this relationship was reversed by increasing CO<sub>2</sub> emissions during the Current Warm Period.

**Plain Language Summary** The East Asian monsoon is characterized by a distinct seasonal reversal of monsoon flow driven by temperature differences between the Pacific Ocean and the East Asian continent. It influences more than 2 billion people around East Asia by regulating the risk of drought or flooding. However, the evolution of the East Asian winter monsoon (EAWM) in the mid-to-late Holocene remains elusive, limiting our understanding of its driving force and projections under climate change. This study analyzed sediment transport dynamics under varying winter monsoons in the North Yellow Sea. It was found that coastal sediments could be transported offshore, and their pathways differed under different strengths of the winter monsoon. Based on the sedimentary records of offshore muddy deposition, the EAWM proxy was extracted, and the wind speed of the EAWM from 4.4 ka was quantitatively reconstructed. A gradual weakening trend during 4.4–0.7 ka and a dramatic strengthening after 0.2 ka were found in the EAWM; the EAWM was negatively related to the temperature on the centennial scale since ~2.0 ka, but this relationship was reversed by an increase in CO<sub>2</sub> emissions since ~1800 CE, indicating a shift in the controlling mechanism.

## 1. Introduction

The East Asian monsoon system plays a fundamental role in transmitting heat and vapor between Eurasia and the surrounding seas, influencing more than 2 billion people in East Asia by regulating the risk of drought or flooding (Turner & Annamalai, 2012). As understanding its past evolution is essential for predicting future conditions, extensive research on East Asian monsoon reconstruction has been conducted in recent decades (e.g., Ding et al., 2017; Sun et al., 2012; Y. Wang et al., 2005; Wen et al., 2016; Xiao et al., 1995). However, unlike the East Asian summer monsoon (EASM), the evolution of the East Asian winter monsoon (EAWM) during the Holocene remains elusive, with a hot debate on whether the EAWM varies in phase with the EASM during the Holocene (Huang et al., 2011; Kang et al., 2020; Steinke et al., 2010; L. Wang et al., 2012). Comparing these reconstructions with modern meteorological data is a feasible way to clarify the above debate; however, few efforts have been made because high-quality sampling and high-precision chronological frameworks covering recent decades are required.

Typically, the EAWM is reconstructed based on its stress force through affecting such as sediment sorting (Ding et al., 2017; Sun et al., 2012), vertical mixing of the water column (Steinke et al., 2010; L. Wang et al., 2012), aquatic surface temperature (Chu et al., 2017; Zhang et al., 2019), and ocean circulation patterns (Huang et al., 2011; Zhao et al., 2019). However, these processes might be disturbed by regional hydrodynamic conditions. For exam-

© 2023. The Authors.

This is an open access article under the terms of the [Creative Commons Attribution-NonCommercial-NoDerivs License](https://creativecommons.org/licenses/by/4.0/), which permits use and distribution in any medium, provided the original work is properly cited, the use is non-commercial and no modifications or adaptations are made.

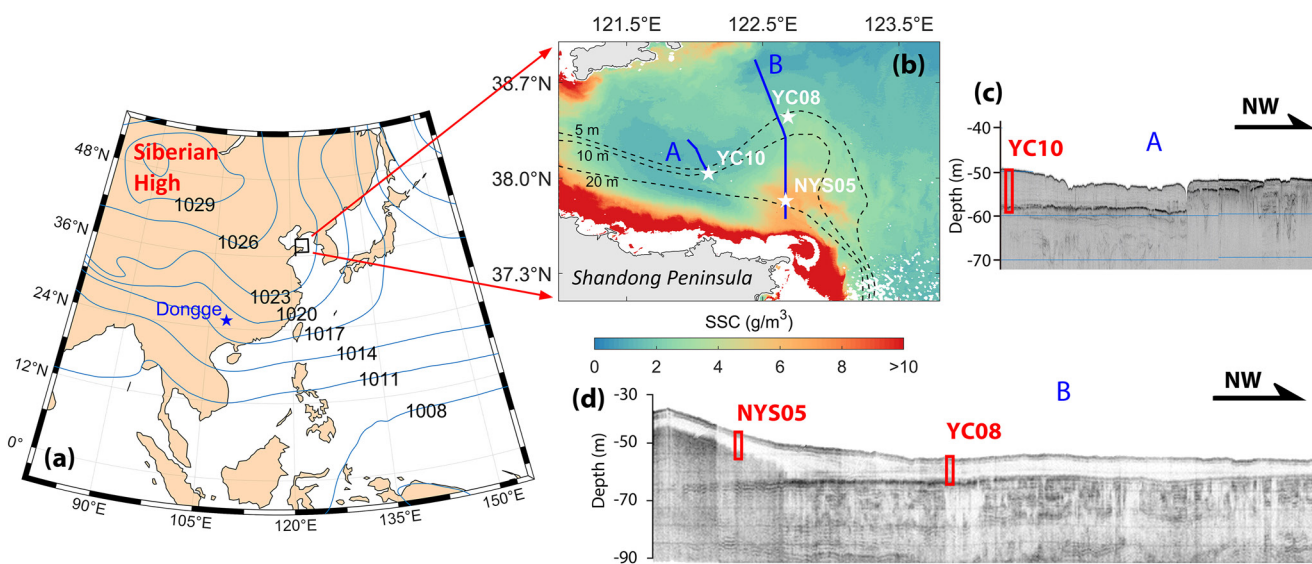


**Figure 1.** (a) Mean barometric pressure of boreal winter in recent 30 yr (1991–2020); (b) Remote sensing derived suspended sediment concentration on 26 January 2019, highlighting cross-front transport from the northeastern cape of the Shandong Peninsula. The 5, 10, and 20 m isopachs of mud patch in the North Yellow sea are marked (Yang & Liu, 2007). Blue lines denote tracks of seismic surveys, and white stars indicate sediment cores. (c and d) Seismic profiles along transects A and B. Transect A was surveyed in this study using a sub-bottom Chirp III sonar profiler. In contrast, transect B is acquired from a previous study (J. P. Liu et al., 2004).

ple, the lithogenic source of the sediments in Huguangyan Maar Lake, a popular place for EAWM reconstruction, is mainly local pyroclastic material (Tian et al., 2010; X. S. Wang et al., 2016; Zhou et al., 2009) rather than the arid areas in northern China (Yancheva et al., 2007), and stalagmite oxygen isotopic records from the northwest coast of the Japanese Islands could also be modulated by the Tsushima Warm Current since the mid-Holocene (Sone et al., 2013). Therefore, it is essential to ensure the reliability of the EAWM proxies.

In this study, offshore sedimentary records in the North Yellow Sea were used to reconstruct the EAWM because this muddy patch is far from large rivers and well preserved in weak tidal fields. Its formation is highly associated with the EAWM (Shi et al., 2022). Driven by winter storms (bursts of the EAWM), coastal sediments of the inner shelf around the Shandong Peninsula are remarkably resuspended, along with elevation in coastal currents during winter storms and the resultant instability of the oceanic front; the suspended coastal sediments could penetrate through the front and be transported offshore from the northeastern cape of the Shandong Peninsula (Shi et al., 2019; Xu et al., 2022) (Figure 1). Thus, variations in the EAWM should be imprinted in the leaked sediment. By comparison with instrumental data from recent decades, the EAWM proxy was extracted, and the wind speed of the EAWM in the mid-to-late Holocene was quantitatively reconstructed at a high resolution (~5 yr).

## 2. Materials and Methods

### 2.1. Sampling and Testing

Sediment cores YC08 (122.10°E, 38.03°N, ~50 m water depth; 510 cm in length) and YC10 (122.69°E, 38.45°N, ~55 m water depth; 544 cm in length) were collected using a gravity sampler in June 2016, and core NYS05 (122.67°E, 37.83°N, ~45 m water depth; 545 cm in length) was collected in July 2020. Sediment cores were sampled at 0.25 and 0.5 cm intervals for the top 44 cm and the rest of core NYS05, respectively, and at 2 cm intervals for cores YC08 and YC10. The samples were soaked in 0.05 mol L<sup>-1</sup> (NaPO<sub>3</sub>)<sub>6</sub> for 24 hr before analysis using a laser particle analyzer (Mastersizer 2000, Malvern Panalytical, UK).

Two isotopic dating methods were used to establish age control for core NYS05 (Tables S1 and S2 in the Supporting Information S1). First, the activity of <sup>210</sup>Pb was measured using alpha spectrometry (Alpha Ensemble, ORTEC, US) to provide a decadal age model of the upper core. A constant rate of <sup>210</sup>Pb supply model was used to determine the deposition rate. The centennial to the millennial chronological framework was determined using radiocarbon dating of the foraminifera/shell. The AMS <sup>14</sup>C ages were calculated as the number of calendar years before the present (set as 1950 CE) using the Marine13 curve. The regional carbon reservoir was set to

$139 \pm 59$  yr (Southon et al., 2002). The age–depth model was established using Bayesian statistics in the Undatable software (Lougheed & Obrochta, 2019).

## 2.2. Model Setup and Configurations

A numerical model based on the Regional Ocean Modeling System (ROMS) was applied to explore the dynamics of cross-front transport around the Shandong Peninsula under winter storms of different strengths. The model domain covers the Bohai and Yellow Seas, ranging from 30°N to 42°N latitude and 117°E to 128°E longitude. The horizontal resolution was approximately 3 km, with 20 vertical layers in sigma coordinates. The model bathymetry was interpolated from the 15-arc-second resolution topographic data of the General Bathymetric Chart of the Oceans (<https://www.gebco.net>). Atmospheric forcing data were interpolated from the European Center for Medium-Range Weather Forecasts (<https://www.ecmwf.int>) ERA5 data with 0.25° spatial resolution and a 3-hr time interval. The initial conditions and two open boundary conditions (south and east, at a frequency of every 12 hr) were obtained from HYCOM + NCODA Global 1/12° analysis data (GLBy0.08/expt\_93.0, <https://www.hycom.org>), including three-dimensional temperature, salinity, and subtidal current fields. Eight principal tidal constituents (M2, S2, N2, K2, K1, O1, P1, and Q1), including sea surface tidal elevation and barotropic tidal currents derived from the TPX09 tidal model (Egbert & Erofeeva, 2002; Engels and van Geel, 2012), are used as tidal forcing along the open boundaries. The model results were validated by comparing them with observed time-series data from coastal stations in the Yellow and Bohai Seas at the hourly tidal sea level, vertically averaged current speed, current direction, and satellite-derived sea surface temperature. Details of the model results and model validation have been reported by Xu et al. (2022).

## 3. Results

### 3.1. Cross-Front Transport Under Different Strengths of Winter Storms

According to the wind data of the Chengchantou Meteorological Station at the northeastern cape of the Shandong Peninsula during 1973–2020, northwesterly wind prevails the North Yellow Sea during the winter (December to March), burst of northwesterly strong wind (>5 m/s, lasting for at least 24 hr) is defined as winter storm. The wind speed of winter storms ranges from 6 to 16 m/s, with the highest frequency at approximately 9 m/s, winter storms can last more than 10 days with the highest frequency at approximately 1.5 days (Figure S1 in the Supporting Information S1).

Different pathways of cross-front transport around the Shandong Peninsula were captured by remote sensing-derived suspended sediment concentrations (Figures 2a and 2b), and their dynamics under different strengths of winter storms were explored using a numerical model based on ROMS (Figure S2 in the Supporting Information S1). The results show that under a relatively weak winter storm (8 m/s, lasting for 2 days, for example), coastal material can penetrate through the front from the northern side of the Shandong Peninsula and move northward when the winter storm recedes (Figure 2c), which is consistent with the cross-front transport shown in Figure 2a and numbered path 1. However, when the winter storm strengthened its wind speed and/or duration (Figure S2 in the Supporting Information S1), the site of cross-front transport moved southeastward. The leaked tracers moved northwestward (12 m/s, lasting for 5 days, e.g., Figure 2d) and numbered path 2, which was also captured by the suspended sediment concentration in Figure 2b.

As clinofolds around the Shandong Peninsula are built by the alongshore transport of Yellow River sediment (J. P. Liu et al., 2004), sediments in coastal areas tend to be finer when moving offshore (Qiao et al., 2017). Presumably, the grain size of the leaked sediment from different transport paths should differ because of the diverse depths and offshore distances between paths 1 and 2. This assumption was verified by the grain size-frequency distribution of the sediment cores collected along the two paths. Core YC08 is located in path 2, its sediments are finer, and a unimodal distribution characterizes its grain size frequency since the highstand (Figure 2e). Core YC10 is located in path 1. Its sediments are coarser and show bimodal features since the highstand (Figure 2f). Core NYS05 could capture sediment leaking from both paths. Its grain size-frequency pattern is thus intermediate between the above two types but has greater fluctuations (Figure 2g).

Although the signal of winter storms in offshore distal mud in shelf seas of eastern China could be covered by the Yellow Sea Warm Current through controlling flux of the cross-front transport (Shi et al., 2022), sediment

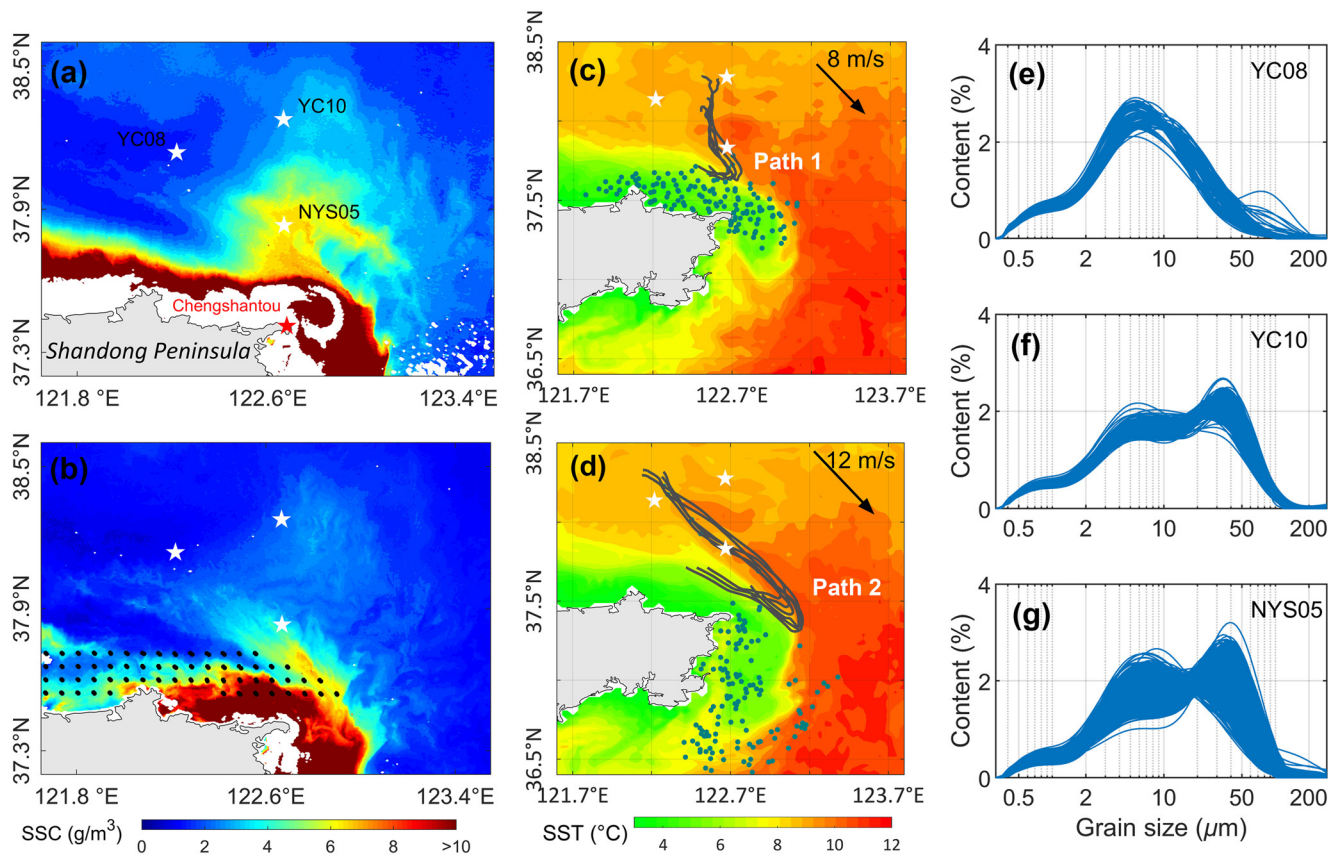


**Figure 2.** (a and b) Cross-front sediment transport revealed by suspended sediment concentration under different strengths of winter storms on 1 and 26 January 2019, respectively. Black circles in the northern coastal area of the Shandong Peninsula are the initial location of the tracers to track material transport during winter storms in a validated numerical model based on the Regional Ocean Modeling System. (c and d) Modeled results showing cross-front transport around the Shandong Peninsula under different strengths of winter storms. Green circles denote the location of the tracers after winter storms, and gray lines show tracks of particles that can penetrate through the front from the northeastern side of the Shandong Peninsula. (e–g) Frequency distribution of grain size at sediment cores for the layers during the highstand (Figure S3 in the Supporting Information S1).

composition in core NYS05 is not likely influenced by this process, because (a) leaked sediments from coastal areas do not suffer long-term transport (sorting) before reaching the site of core NYS05, unlike the conditions in Shi et al. (2022); (b) flux of offshore transport from both paths (1 and 2) is equivalently influenced by the Yellow Sea Warm Current, that is, sediment flux from both paths would be promoted when the Yellow Sea Warm Current enhances, sediment composition in core NYS05 is controlled by the relative occurrence frequency between the two paths, which is determined by the strength of winter storms. Under a stronger wind, more fine sediments (0–20  $\mu\text{m}$ ) will be transported offshore along path 2, and the proportion of fine sediments in core NYS05 would thus be promoted. Therefore, the proportion of fine sediment could be a potential proxy of winter storms, which, however, is different from the common view in previous paleoclimate studies that coarser sediment, such as 20–100  $\mu\text{m}$  in this study, reflects a stronger winter storm.

### 3.2. Quantitative Reconstruction of the EAWM

The EAWM in the North Yellow Sea is characterized by northwesterly wind, its intermittent burst, defined as winter storms, accounts for 44.2% of the winter months (December to March) according to meteorological data of the Chengshantou Station. As cross-front transport around the Shandong Peninsula is triggered by winter storms, strengths of winter storms could be imprinted in the leaked sediment. Additionally, because the EAWM varied in a manner similar to winter storms (Figure 3a), its history could also be reconstructed from core NYS05.

The chronological framework of core NYS05 on a decadal scale was determined using  $^{210}\text{Pb}$  (Figure S4 in the Supporting Information S1); the average deposition rate for the layer after 1973 was  $\sim 0.35$  cm/yr. By comparison

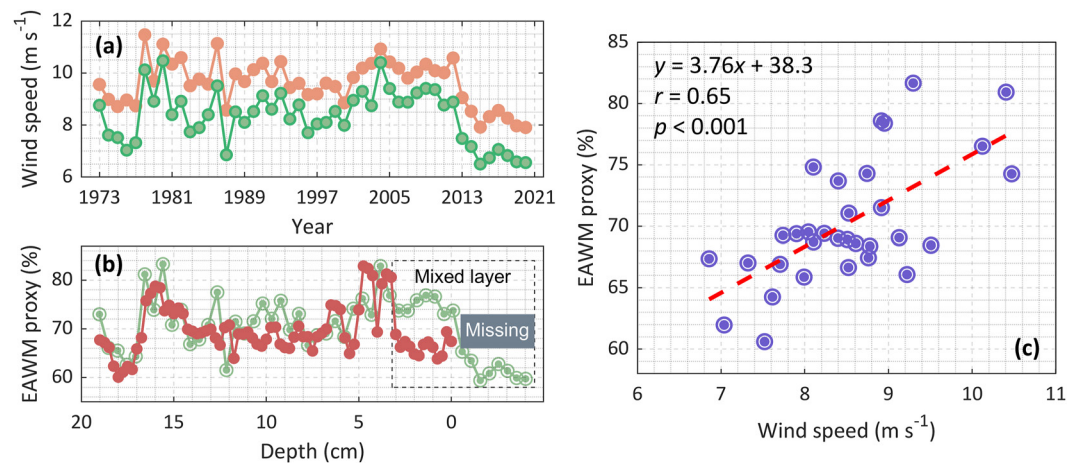


**Figure 3.** (a) Mean speed of northwesterly wind (green) and winter storm (orange) during December to March recorded at the Chengshantou meteorological station for 1973–2020. (b) The proportion of fine fraction (0–20  $\mu\text{m}$ ) in core NYS05 (red) served as the East Asian winter monsoon (EAWM) proxy, and the calculated EAWM proxy (green) is based on wind speed in panel (a) according to the relationship in panel (c). (c) Correlation between the wind speed of the EAWM during 1973–2006 and proportion of fine fraction in the 19–3.5 cm layer.

with the wind series, the age–depth model of core NYS05 was slightly adjusted (Figure 3b). After the adjustment, a high degree of consistency was found between wind speed during 1973–2006 and proportion of fine fraction (0–20  $\mu\text{m}$ ) in 19–3.5 cm depth, and their coefficient could reach 0.65 (Figure 3c); however, huge divergence was detected in the shallow part, that is, the wind gradually weakened since 2007, but the proportion of fine fraction kept relatively steady in the shallow 3.5 cm. Therefore, we speculated that the shallow layer (7.5 cm thick) was disturbed during sampling and the surface layer (approximately 4 cm thick) was lost. The following evidence supports this speculation. (a) According to the correlation between the EAWM proxy and wind strength in Figure 3c, the expected proportion of the fine fraction based on wind strength during 1973–2020 was calculated (Figure 3b), and it was found that the mean value of the expected EAWM proxy in the mixed layer is 68.0%, which is similar to that of the retained mixed layer (0–3.3 cm deep, 64.5%). (b)  $^{210}\text{Pb}$  activity in the surface layer was much lower than in the adjacent underlying layers (Figure S4 in the Supporting Information S1; Table S1 in the Supporting Information S1), indicating that it was highly disturbed. This disturbance degree (7.5 cm thick) and collection rate (99.3%) are generally acceptable when drilling a 5.45 m-length sediment core.

The linear relationship in Figure 3c is applied to quantitatively reconstruct the EAWM on the millennial scale, considering the facts that (a) the depositional environment was relatively steady since the mid-Holocene because of little variability of sea-level; (b) although flux of cross-front transport is associated with the strength of the continental circulations and they were found to be variable even since the highstand (Jia et al., 2019; L. B. Wang et al., 2011; Zhang et al., 2019), sediment composition in core NYS05 was regulated by the relative contribution between the two paths; (c) despite frequent migration of the Yellow River (at least 10 times since  $\sim 7.0$  ka [Xue, 1993]) and variation of riverine sediment discharge (increased more than 10 times from 0.23 Gt/yr at 1.4 ka to 1.56 Gt/yr at 1855 CE and reverted to pristine levels in recent decades [Wu et al., 2020]) in history, coastal sediment around the Shandong Peninsula is relative homogenous in grain size (J. Liu et al., 2007), because along-shore sediment transport in shelf seas of eastern China mostly takes place in winter due to increase of resuspension and coastal current under energetic winter monsoon, and the Yellow River-derived sediment would suffered intensively sorting before reaching the northern coastal areas of the Shandong Peninsula.

According to the depth–age model based on AMS  $^{14}\text{C}$ , the 545 cm-length marine sequence extends the EAWM history back to 4.4 ka (Figure S4 in the Supporting Information S1). As the core was subsampled at an interval of 0.5 cm on a millennial scale, the EAWM was reconstructed at a high resolution of approximately 5 yr. The result shows that the EAWM in the North Yellow Sea generally decreased from  $\sim 8.5$  to  $\sim 6.5$  m/s during 4.4–0.8 ka and gradually increased to  $\sim 9$  m/s after 0.2 ka with multi-time scale fluctuations (Figure 4a). Additionally, remarkable centennial-scale fluctuations were found since 2.0 ka; the EAWM was weak during 1.5–0.6 ka, especially at the Medieval Warm Period (MWP), relatively strong at the Little Ice Age (LIA), and dramatically strengthened at the Current Warm Period (CWP).

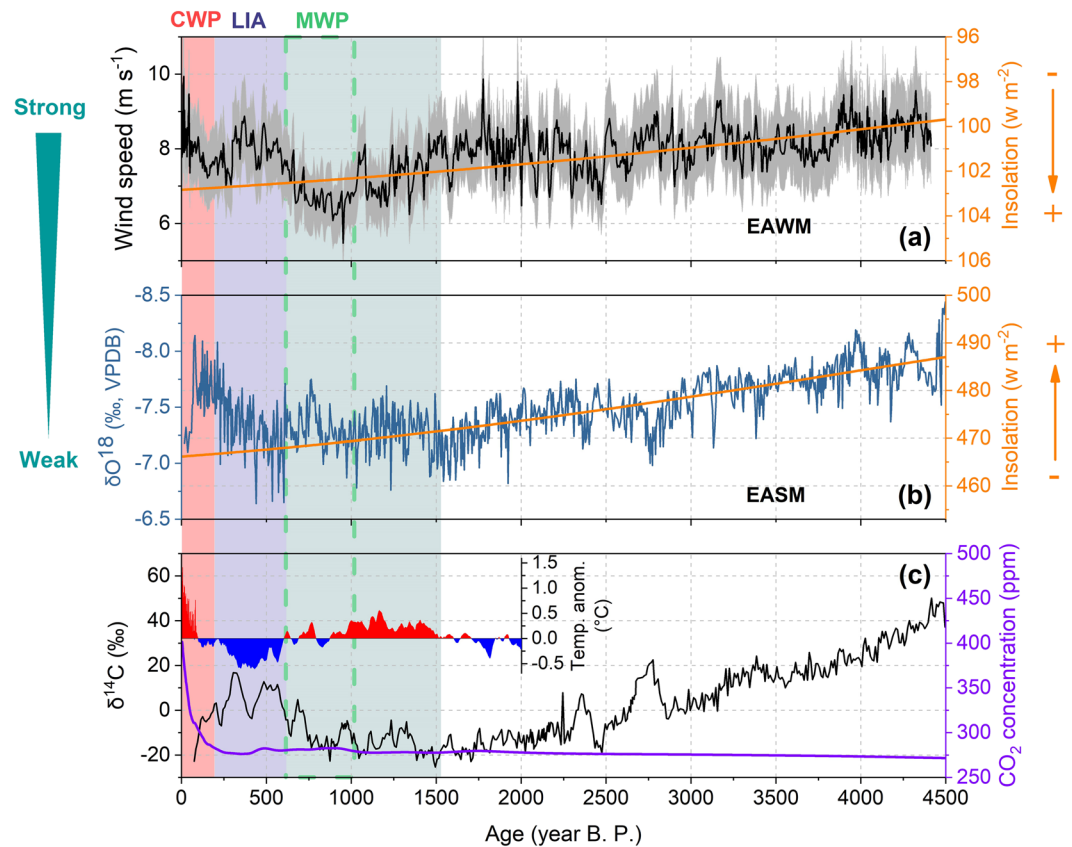


**Figure 4.** (a) Wind speed of the East Asian winter monsoon (EAWM) revealed from core NYS05 (black line) with 95% confidence interval, along with the solar insolation (orange line) at 50°N in mid-January (Berger & Loutre, 1991). (b) Evolution of the East Asian summer monsoon (EASM) imprinted in Dongge stalagmite (Y. Wang et al., 2005), along with the solar insolation at 50°N in mid-July (orange line). (c) Time serials of radiocarbon ( $\delta^{14}\text{C}$ ) of tree rings (Stuiver et al., 1998), carbon dioxide concentration (Köhler et al., 2017), and global temperature anomaly (blue, cool; red, warm) (Loehle & McCulloch, 2008). The Medieval Warm Period (MWP), Little Ice Age (LIA), and Current Warm Period (CWP) are highlighted. The present is defined as 2020 CE.

#### 4. Discussion

Our reconstructed EAWM dating back to 4.4 ka varies in a highly consistent manner compared to a well-respected high-resolution ( $\sim 5$  yr) EASM record in Dongge stalagmite, southwestern China (Figures 4a and 4b), indicating that the same force might drive them on the sub-orbital scale. The East Asian Monsoon is characterized by a distinct seasonal reversal of monsoon flow, driven by temperature differences between the Pacific Ocean and the East Asian region (Li & Yanai, 1996). The small heat capacity of the continent, which results in stronger seasonality in temperature (barometric pressure) relative to the sea, makes the continent more sensitive to solar insolation (Hu et al., 2012). Accompanied by a decrease in summer insolation and an increase in winter insolation in the Northern hemisphere since 4.4 ka (Figures 4a and 4b), a smaller temperature (barometric pressure) contrast between the continent and sea limited the seasonal meridional migration of the Intertropical Convergence Zone, through which both the East Asian winter and summer monsoons weakened. Our analysis confirms the role of solar radiation in driving the East Asian monsoon at the sub-orbital scale during the Holocene. Compared with other reconstruction works, the same conclusion was also obtained from tropical aqueous environments (Huang et al., 2011; Steinke et al., 2010; L. Wang et al., 2012), suggesting no zonal difference between the two sites. However, distinct results appear in the loess deposits (Kang et al., 2020), which might be due to their limited applicability in the East Asian monsoon reconstruction because they were subaerial and might not be well preserved for millennial-scale reconstruction.

In addition, centennial-scale oscillations were found in the EAWM, especially from  $\sim 2.0$  ka, when the MWP, LIA, and CWP occurred sequentially (Figure 4a). At present, although the underlying mechanism for these

climatic oscillations remains ambiguous, some key controlling factors have been identified, such as solar activity for the LIA and increased CO<sub>2</sub> emissions for the CWP (Figure 3c). The period since ~2.0 ka is focused on. A negative relationship between the strength of the EAWM and temperature was found, but this relationship was reversed during the CWP, which might indicate a shift in the controlling mechanism. Global warming in the CWP has been attributed to a sharp increase in atmospheric CO<sub>2</sub> concentrations, particularly after 0.1 ka when the temperature was much higher than that of the MWP (Figure 4c). Under warming conditions, seawater in the North Atlantic is fresher because of an increase in ice melting, leading to a slowdown of the Atlantic meridional overturning circulation (Couldrey et al., 2023; Haskins et al., 2019), which reduces global northward ocean heat transport at all latitudes. This was partially, but not entirely, offset by an increase in atmospheric heat transport. Consequently, climate warming is inhibited at high latitudes relative to low latitudes, and an increasing meridional temperature gradient is created (Sun et al., 2012), which enhances the EAWM and suppresses the EASM (Figures 4a and 4b). Additionally, as the stalagmite-derived EASM is a proxy for precipitation rather than wind speed, it did not strictly follow the variations in the EAWM.

The East Asian climate is influenced by El Niño and the Southern Oscillation (ENSO), which modify atmospheric circulation over the western North Pacific region. This process can be modulated by the phase of the Pacific Decadal Oscillations (PDO) and Atlantic Multi-decadal Oscillations (AMO), according to instrumental data (Geng et al., 2017; Kim et al., 2017; Sandeep et al., 2022). Based on spectral analysis (Figure S5 in the Supporting Information S1), decadal cycles in the East Asian Monsoon likely confirm the role of the AMO and PDO in controlling the East Asian climate. However, unlike the PDO signal (~20- to 30-yr cycles) (Latif & Barnett, 1996; Minobe, 1999) could be found in both the winter and summer monsoons, the AMO signal (~55- to 70-yr cycles) (Knudsen et al., 2011) only appeared in the winter monsoon. This discrepancy helps clarify the AMO's influence on the East Asian climate. Therefore, the Rossby wave train from the subtropical North Atlantic and propagating across the Eurasian continent to northeast Asia is preferred because if the role of the AMO in regulating the East Asian climate is through controlling the northwest Pacific anticyclone, multi-decadal cycles should also be recorded in the EASM.

## 5. Conclusions

The dynamics of offshore transport in the North Yellow Sea were explored using a numerical model, and it was found that the grain size of leaked sediment from the coastal area could imprint the strength of the EAWM. By comparison with instrumental data, the EAWM proxy was extracted, and the wind speed of the EAWM since 4.4 ka was reconstructed at a high resolution (~5 yr). The results showed that the EAWM gradually weakened from the mid-to-late Holocene, sharing a trend similar to the EASM. The millennial-scale weakening trend in the EAWM was likely regulated by solar insolation. A negative relationship between the EAWM and temperature on the centennial scale was found in the late Holocene. Still, this relationship was reversed by increasing CO<sub>2</sub> emissions at the CWP (since ~1800 CE) through weakening the Atlantic meridional overturning circulation.

## Data Availability Statement

Wind data of the Changshantou Meteorological Station is acquired from the NOAA (<https://www.ncei.noaa.gov/maps/hourly/>). The reconstructed wind speed of the EAWM is available at supporting information (Data Set S1).

## References

- Berger, A., & Loutre, M. F. (1991). Insolation values for the climate of the last 10 million years. *Quaternary Science Reviews*, 10(4), 297–317. [https://doi.org/10.1016/0277-3791\(91\)90033-q](https://doi.org/10.1016/0277-3791(91)90033-q)
- Chu, G., Sun, Q., Zhu, Q., Shan, Y., Shang, W., Ling, Y., et al. (2017). The role of the Asian winter monsoon in the rapid propagation of abrupt climate changes during the last deglaciation. *Quaternary Science Reviews*, 177, 120–129. <https://doi.org/10.1016/j.quascirev.2017.10.014>
- Couldrey, M. P., Gregory, J. M., Dong, X., Garuba, O., Haak, H., Hu, A., et al. (2023). Greenhouse-gas forced changes in the Atlantic meridional overturning circulation and related worldwide sea-level change. *Climate Dynamics*, 60(7–8), 1–37. <https://doi.org/10.1007/s00382-022-06386-y>
- Ding, Z., Liu, T., Rutter, N. W., Yu, Z., Guo, Z., & Zhu, R. (2017). Ice-volume forcing of East Asian winter monsoon variations in the past 800,000 years. *Quaternary Research*, 44(2), 149–159. <https://doi.org/10.1006/qres.1995.1059>
- Egbert, G. D., & Erofeeva, S. Y. (2002). Efficient inverse modeling of barotropic ocean tides. *Journal of Atmospheric and Oceanic Technology*, 19(2), 183–204. [https://doi.org/10.1175/1520-0426\(2002\)019<0183:Eimobo>2.0.Co;2](https://doi.org/10.1175/1520-0426(2002)019<0183:Eimobo>2.0.Co;2)
- Engels, S., & van Geel, B. (2012). The effects of changing solar activity on climate: Contributions from palaeoclimatological studies. *Journal of Space Weather and Space Climate*, 2, A09. <https://doi.org/10.1051/swsc/2012009>

## Acknowledgments

This studied was jointly funded by the National Natural Science Foundation of China (Nos. 42106158, 42276170), the Fundamental Research Funds for the Central Universities (Nos. 14380092, 14380100), and Frontiers Science Center for Critical Earth Material Cycling, Nanjing University.

- Geng, X., Zhang, W., Stuecker, M. F., Liu, P., Jin, F.-F., & Tan, G. (2017). Decadal modulation of the ENSO–East Asian winter monsoon relationship by the Atlantic Multidecadal Oscillation. *Climate Dynamics*, *49*(7), 2531–2544. <https://doi.org/10.1007/s00382-016-3465-0>
- Haskins, R. K., Oliver, K. I. C., Jackson, L. C., Wood, R. A., & Drijfhout, S. S. (2019). Temperature domination of AMOC weakening due to freshwater hosing in two GCMs. *Climate Dynamics*, *54*(12), 273–286. <https://doi.org/10.1007/s00382-019-04998-5>
- Hu, B. Q., Yang, Z. S., Zhao, M. X., Saito, Y., Fan, D. J., & Wang, L. B. (2012). Grain size records reveal variability of the East Asian winter monsoon since the Middle Holocene in the Central Yellow Sea mud area, China. *Science China Earth Sciences*, *55*(10), 1656–1668. <https://doi.org/10.1007/s11430-012-4447-7>
- Huang, E. Q., Tian, J., & Steinke, S. (2011). Millennial-scale dynamics of the winter cold tongue in the southern South China Sea over the past 26 ka and the East Asian winter monsoon. *Quaternary Research*, *75*(1), 196–204. <https://doi.org/10.1016/j.yqres.2010.08.014>
- Jia, Y. H., Li, D. W., Yu, M., Zhao, X. C., Xiang, R., Li, G. X., et al. (2019). High- and low-latitude forcing on the south Yellow Sea surface water temperature variations during the Holocene. *Global and Planetary Change*, *182*, 103025. <https://doi.org/10.1016/j.gloplacha.2019.103025>
- Kang, S. G., Du, J. H., Wang, N., Dong, J. B., Wang, D., Wang, X. L., et al. (2020). Early Holocene weakening and mid- to late Holocene strengthening of the East Asian winter monsoon. *Geology*, *48*(11), 1043–1047. <https://doi.org/10.1130/G47621.1>
- Kim, J. W., An, S. I., Jun, S. Y., Park, H. J., & Yeh, S. W. (2017). ENSO and East Asian winter monsoon relationship modulation associated with the anomalous northwest Pacific anticyclone. *Climate Dynamics*, *49*(4), 1157–1179. <https://doi.org/10.1007/s00382-016-3371-5>
- Knudsen, M. F., Seidenkrantz, M. S., Jacobsen, B. H., & Kuijpers, A. (2011). Tracking the Atlantic Multidecadal Oscillation through the last 8,000 years. *Nature Communications*, *2*(1), 1–8. <https://doi.org/10.1038/ncomms1186>
- Köhler, P., Nehrbass-Ahles, C., Schmitt, J., Stocker, T. F., & Fischer, H. (2017). A 156 kyr smoothed history of the atmospheric greenhouse gases CO<sub>2</sub>, CH<sub>4</sub>, and N<sub>2</sub>O and their radiative forcing. *Earth System Science Data*, *9*(1), 363–387. <https://doi.org/10.5194/essd-9-363-2017>
- Latif, M., & Barnett, T. P. (1996). Decadal climate variability over the North Pacific and North America: Dynamics and predictability. *Journal of Climate*, *9*(10), 2407–2423. [https://doi.org/10.1175/1520-0442\(1996\)009<2407:Dcvotn>2.0.Co;2](https://doi.org/10.1175/1520-0442(1996)009<2407:Dcvotn>2.0.Co;2)
- Li, C., & Yanai, M. (1996). The onset and interannual variability of the Asian summer monsoon in relation to land–sea thermal contrast. *Journal of Climate*, *9*(2), 358–375. [https://doi.org/10.1175/1520-0442\(1996\)009<0358:Toaivo>2.0.Co;2](https://doi.org/10.1175/1520-0442(1996)009<0358:Toaivo>2.0.Co;2)
- Liu, J., Saito, Y., Wang, H., Yang, Z. G., & Nakashima, R. (2007). Sedimentary evolution of the Holocene subaqueous clinoform off the Shandong Peninsula in the Yellow Sea. *Marine Geology*, *236*(3–4), 165–187. <https://doi.org/10.1016/j.margeo.2006.10.031>
- Liu, J. P., Milliman, J. D., Gao, S., & Cheng, P. (2004). Holocene development of the Yellow River's subaqueous delta, North Yellow Sea. *Marine Geology*, *209*(1–4), 45–67. <https://doi.org/10.1016/j.margeo.2004.06.009>
- Loehle, C., & McCulloch, J. H. (2008). Correction to: A 2000-year global temperature reconstruction based on non-tree ring proxies. *Energy & Environment*, *19*(1), 93–100. <https://doi.org/10.1260/095830507782616797>
- Lougheed, B. C., & Obrochta, S. P. (2019). A rapid, deterministic age-depth modeling routine for geological sequences with inherent depth uncertainty. *Paleoceanography and Paleoclimatology*, *34*(1), 122–133. <https://doi.org/10.1029/2018pa003457>
- Minobe, S. (1999). Resonance in bidecadal and pentadecadal climate oscillations over the North Pacific: Role in climatic regime shifts. *Geophysical Research Letters*, *26*(7), 855–858. <https://doi.org/10.1029/1999gl900119>
- Qiao, S. Q., Shi, X. F., Wang, G. Q., Zhou, L., Hu, B. Q., Hu, L. M., et al. (2017). Sediment accumulation and budget in the Bohai Sea, Yellow Sea and East China Sea. *Marine Geology*, *390*, 270–281. <https://doi.org/10.1016/j.margeo.2017.06.004>
- Sandeep, N., Swapna, P., Krishnan, R., Farneti, R., Kucharski, F., Modi, A., et al. (2022). On the weakening association between South Asian Monsoon and Atlantic Multidecadal Oscillation. *Climate Dynamics*, *59*(9–10), 2531–2547. <https://doi.org/10.1007/s00382-022-06224-1>
- Shi, Y., Gao, J. H., Sheng, H., Du, J., Jia, J. J., Wang, Y. P., et al. (2019). Cross-front sediment transport induced by quick oscillation of the Yellow Sea warm current: Evidence from the sedimentary record. *Geophysical Research Letters*, *46*(1), 226–234. <https://doi.org/10.1029/2018gl080751>
- Shi, Y., Xu, X., Sheng, H., Lv, J., Zhang, S., & Gao, J. (2022). Neglected role of continental circulation in cross-shelf sediment transport: Implications for paleoclimate reconstructions. *Marine Geology*, *443*, 106703. <https://doi.org/10.1016/j.margeo.2021.106703>
- Sone, T., Kano, A., Okumura, T., Kashiwagi, K., Hori, M., Jiang, X. Y., & Shen, C. C. (2013). Holocene stalagmite oxygen isotopic record from the Japan Sea side of the Japanese Islands, as a new proxy of the East Asian winter monsoon. *Quaternary Science Reviews*, *75*, 150–160. <https://doi.org/10.1016/j.quascirev.2013.06.019>
- Southon, J., Kashgarian, M., Fontugne, M., Metivier, B., & Yim, W. W. S. (2002). Marine reservoir corrections for the Indian Ocean and South-east Asia. *Radiocarbon*, *44*(1), 167–180. <https://doi.org/10.1017/S003822200064778>
- Steinke, S., Mohtadi, M., Groeneveld, J., Lin, L. C., Lowemark, L., Chen, M. T., & Rendle-Buhring, R. (2010). Reconstructing the southern South China Sea upper water column structure since the Last Glacial Maximum: Implications for the East Asian winter monsoon development. *Paleoceanography*, *25*(2). <https://doi.org/10.1029/2009pa001850>
- Stuiver, M., Reimer, P. J., & Braziunas, T. F. (1998). High-precision radiocarbon age calibration for terrestrial and marine samples. *Radiocarbon*, *40*(3), 1127–1151. <https://doi.org/10.1017/S003822200019172>
- Sun, Y. B., Clemens, S. C., Morrill, C., Lin, X. P., Wang, X. L., & An, Z. S. (2012). Influence of Atlantic meridional overturning circulation on the East Asian winter monsoon. *Nature Geoscience*, *5*(1), 46–49. <https://doi.org/10.1038/Ngeo1326>
- Tian, J., Huang, E. Q., & Pak, D. K. (2010). East Asian winter monsoon variability over the last glacial cycle: Insights from a latitudinal sea-surface temperature gradient across the South China Sea. *Palaeogeography, Palaeoclimatology, Palaeoecology*, *292*(1–2), 319–324. <https://doi.org/10.1016/j.palaeo.2010.04.005>
- Turner, A. G., & Annamalai, H. (2012). Climate change and the South Asian summer monsoon. *Nature Climate Change*, *2*(8), 587–595. <https://doi.org/10.1038/Nclimate1495>
- Wang, L., Li, J., Lu, H., Gu, Z., Rioual, P., Hao, Q., et al. (2012). The East Asian winter monsoon over the last 15,000 years: Its links to high-latitudes and tropical climate systems and complex correlation to the summer monsoon. *Quaternary Science Reviews*, *32*, 131–142. <https://doi.org/10.1016/j.quascirev.2011.11.003>
- Wang, L. B., Yang, Z. S., Zhang, R. P., Fan, D. J., Zhao, M. X., & Hu, B. Q. (2011). Sea surface temperature records of core ZY2 from the central mud area in the South Yellow Sea during last 6200 years and related effect of the Yellow Sea Warm Current. *Chinese Science Bulletin*, *56*(15), 1588–1595. <https://doi.org/10.1007/s11434-011-4442-y>
- Wang, X. S., Chu, G. Q., Sheng, M., Zhang, S. Q., Li, J. H., Chen, Y., et al. (2016). Millennial-scale Asian summer monsoon variations in South China since the last deglaciation. *Earth and Planetary Science Letters*, *451*, 22–30. <https://doi.org/10.1016/j.epsl.2016.07.006>
- Wang, Y., Cheng, H., Edwards, R. L., He, Y., Kong, X., An, Z., et al. (2005). The Holocene Asian monsoon: Links to solar changes and North Atlantic climate. *Science*, *308*(5723), 854–857. <https://doi.org/10.1126/science.1106296>
- Wen, X., Liu, Z., Wang, S., Cheng, J., & Zhu, J. (2016). Correlation and anti-correlation of the East Asian summer and winter monsoons during the last 21,000 years. *Nature Communications*, *7*(1), 11999. <https://doi.org/10.1038/ncomms11999>
- Wu, X., Wang, H. J., Bi, N. S., Saito, Y., Xu, J. P., Zhang, Y., et al. (2020). Climate and human battle for dominance over the Yellow River's sediment discharge: From the Mid-Holocene to the Anthropocene. *Marine Geology*, *425*, 106188. <https://doi.org/10.1016/j.margeo.2020.106188>



- Xiao, J., Porter, S. C., An, Z. S., Kumai, H., & Yoshikawa, S. (1995). Grain-size of quartz as an indicator of winter monsoon strength on the loess plateau of central China during the last 130,000-yr. *Quaternary Research*, *43*(1), 22–29. <https://doi.org/10.1006/qres.1995.1003>
- Xu, X. M., Gao, J. H., Shi, Y., Wu, X. D., Lv, J. X., Zhang, S., et al. (2022). Cross-front transport triggered by winter storms around the Shandong Peninsula, China. *Frontiers in Marine Science*, *9*, 975504. <https://doi.org/10.3389/fmars.2022.975504>
- Xue, C. T. (1993). Historical changes in the Yellow-River Delta, China. *Marine Geology*, *113*(3–4), 321–330. [https://doi.org/10.1016/0025-3227\(93\)90025-Q](https://doi.org/10.1016/0025-3227(93)90025-Q)
- Yancheva, G., Nowaczyk, N. R., Mingram, J., Dulski, P., Schettler, G., Negendank, J. F., et al. (2007). Influence of the intertropical convergence zone on the East Asian monsoon. *Nature*, *445*(7123), 74–77. <https://doi.org/10.1038/nature05431>
- Yang, Z. S., & Liu, J. P. (2007). A unique Yellow River-derived distal subaqueous delta in the Yellow Sea. *Marine Geology*, *240*(1–4), 169–176. <https://doi.org/10.1016/j.margeo.2007.02.008>
- Zhang, Y. C., Zhou, X., He, Y. X., Jiang, Y. Q., Liu, Y., Xie, Z. Q., et al. (2019). Persistent intensification of the Kuroshio Current during late Holocene cool intervals. *Earth and Planetary Science Letters*, *506*, 15–22. <https://doi.org/10.1016/j.epsl.2018.10.018>
- Zhao, D. B., Wan, S. M., Song, Z. Y., Gong, X., Zhai, L. N., Shi, X. F., & Li, A. C. (2019). Asynchronous variation in the quaternary East Asian winter monsoon associated with the tropical Pacific ENSO-like system. *Geophysical Research Letters*, *46*(12), 6955–6963. <https://doi.org/10.1029/2019gl083033>
- Zhou, H. Y., Wang, B. S., Guan, H. Z., Lai, Y. J., You, C. F., Wang, J. L., & Yang, H. J. (2009). Constraints from strontium and neodymium isotopic ratios and trace elements on the sources of the sediments in Lake Huguang Maar. *Quaternary Research*, *72*(2), 289–300. <https://doi.org/10.1016/j.yqres.2009.06.005>